ERJ open research
THE BEST IN OPEN ACCESS BASIC, TRANSLATIONAL & CLINICAL RESPIRATORY RESEARCH

Early View

Original research article

Suppression of epithelial abnormalities by nintedanib in induced-rheumatoid arthritis-associated interstitial lung disease mouse model

Yoko Miura, Hirotsugu Ohkubo, Akio Niimi, Satoshi Kanazawa

Please cite this article as: Miura Y, Ohkubo H, Niimi A, *et al*. Suppression of epithelial abnormalities by nintedanib in induced-rheumatoid arthritis-associated interstitial lung disease mouse model. *ERJ Open Res* 2021; in press (https://doi.org/10.1183/23120541.00345-2021).

Suppression of epithelial abnormalities by nintedanib in induced-rheumatoid arthritis-associated interstitial lung disease mouse model

Yoko Miura[1], Hirotsugu Ohkubo[2], Akio Niimi[2], and Satoshi Kanazawa[1]

Author affiliations

[1] Department of Neurodevelopmental Disorder Genetics, Nagoya City University Graduate School of Medical Sciences, Nagoya, Japan.

[2] Department of Respiratory Medicine, Allergy and Clinical Immunology, Nagoya City University Graduate School of Medical Sciences, Nagoya, Japan.

Address correspondence to Satoshi Kanazawa, PhD, Department of Neurodevelopmental Disorder Genetics, Nagoya City University Graduate School of Medical Sciences, 1 Kawasumi, Mizuho-cho, Mizuho-ku, Nagoya, 467-8601, Japan

E-mail: kanas@med.nagoya-cu.ac.jp Tel number: 81-52-853-8205

Abstract

Rheumatoid arthritis-associated interstitial lung disease (RA-ILD) is relevant for the prognosis in patients with RA. Nintedanib, which inhibits both receptor and non-receptor type tyrosine kinases, is an antifibrotic drug for the treatment of progressive fibrosing ILDs, such as idiopathic pulmonary fibrosis and systemic sclerosis-associated interstitial lung disease. Little is known about the effects of nintedanib on RA-ILD. We examined the characteristics of a novel induced RA-ILD (iRA-ILD) mouse model and the effects of nintedanib on the model.

D1CC×D1BC mice are highly susceptible to arthritogenic antigens, such as bovine type II collagen, resulting in severe inflammatory arthritis. ILD develops after joint inflammation alleviates. Serum surfactant protein D levels were monitored as an ILD marker. Nintedanib was orally administered to iRA-ILD mice for two months.

The iRA-ILD model showed similar symptoms as in patients with RA-ILD. The histopathological features of pulmonary disorder resembled nonspecific interstitial pneumonia, but with metaplastic epithelium. Histopathological analysis revealed that in addition to reducing fibrosis, nintedanib suppressed M2 macrophage polarization and hyperplasia of type 2 alveolar epithelial cells. The metaplastic epithelium acquired invasiveness because of the expression of E-cadherin, MMP7, *Tgf-β*, *Col1a1, Padi2*, and *Padi4*. Moreover, citrullinated peptides were detected in these invasive epithelial cells as well as in the bronchiolar epithelium. Administration of nintedanib reduced the expression of Pad4 and citrullinated peptides and eliminated invasive epithelial cells.

The broad inhibitory effects of nintedanib on tyrosine kinases may contribute to the overall improvement in RA-ILD, including epithelial abnormalities associated with progressive lung fibrosis.

Key words

Rheumatoid arthritis-associated interstitial lung disease, nintedanib, epithelial mesenchymal transition, peptidyl arginine deiminase, citrullination

Introduction

Rheumatoid arthritis (RA) is caused by chronic inflammation of the joints. RA-associated interstitial lung disease (RA-ILD) is a serious extra-articular manifestation of RA. The current prevalence of RA-ILD is approximately 20-50% [1]. In addition, drug-induced lung disease by disease-modifying anti-rheumatic drugs such as methotrexate and leflunomide, presumably affects the onset of RA-ILD. Most RA-ILD is classified as nonspecific interstitial pneumonia (NSIP) and usual interstitial pneumonia (UIP) patterns [2]. The mortality rate of RA-ILD is increasing, even though treatment with biologics has reduced the symptoms of arthritis [3].

The developmental mechanism of RA-ILD is not clear, one of the reasons being the lack of appropriate animal models [4]. For example, in a collagen-induced mouse model, there are no symptoms related to lung disease. SKG mouse is known as a mouse model of RA-ILD, in which infiltration of lymphoid cells and fibrosis develops. The onset of its symptoms is observed in approximately 15% of arthritogenic antigen-treated mice [5]. We previously reported a new murine RA-ILD model, D1CC and D1BC RA mouse model, which expresses human class II transactivator, CIITA, and murine B7.1 in chondrocytes, respectively [6, 7]. Both mice developed chronic inflammatory arthritis with low dose of bovine type II collagen (bColII) immunization. After remission of joint inflammation, we observed ILD without any additional stimuli. Histopathological features in D1CC and D1BC mice are similar to NSIP due to observation of infiltrated lymphoid cells and fibrosis. H_2-treatment improved fibrosis in D1CC mice as an RA-ILD model [8]. In this study, we used D1CC×D1BC transgenic (tg) mice (hereafter named iRA-ILD mouse). D1CC×D1BC tg mice are also susceptible to inhalation injury with bleomycin in the lung. It causes chronic interstitial pneumonia, a pathological feature of honeycombing [9].

Serological features in patients with RA are associated with high levels of serum rheumatoid factor (RF) IgG, IgM, and anti-citrullinated protein/peptide antibody (ACPA), which are risk factors for extra-articular manifestations, including ILD [4]. Combined presence of ACPA and RF leads to severe systemic inflammation and rapid exacerbation of RA [10]. Both serum RF IgG and IgM levels are strongly associated with the development of RA and RA-ILD [11]. These factors may be involved as a shared disease mechanism leading to the development of RA and ILD [2].

Epithelial-mesenchymal transition (EMT) is an active, reversible process associated with embryogenesis, wound healing, cancer metastasis, and fibrosis [12]. Aberrant deposition and remodeling of the extracellular matrix (ECM) has been observed in patients with RA-ILD. Metastatic respiratory epithelia have been observed in the lungs

of patients with IPF [13]. The involvement of these ectopic and hyperplastic cells in fibrosis is not clear, but some of them acquire the ability of EMT [14]. Fibrosis and remodeling failures occur as a result of chronic parenchymal damage. Indeed, hyperplastic respiratory epithelial cells proliferate and migrate in the lung [15]. Recent studies have demonstrated that inhibition or silencing of peptidylarginine deiminase 4 (PAD4) reduces EMT and neutrophil extracellular traps [16]; however, the effect of PAD4 on EMT in cancer cells is controversial [17]. Nevertheless, various tumors, including lung squamous carcinoma express PAD4 and citrullinated peptide, and their function in epithelial cells is less clear [18, 19]. As PAD2 and PAD4 are also involved in EMT, citrullination by PADs may result in tumorigenesis [20].

Nintedanib (BIBF-1120), a drug for patients with progressive fibrosing ILD [21], blocks the ATP-binding pocket of non-receptor tyrosine kinases, such as Src family kinases as well as receptor tyrosine kinases, such as platelet-derived growth factor receptor (PDGFR), fibroblast growth factor receptor (FGFR), and vascular endothelial growth factor receptor (VEGFR) [22-24]. Even though pulmonary fibrosis in SKG mice as an RA-ILD model has a lower incidence (~20%), nintedanib reduced it [25]. Nintedanib inhibited transforming growth factor-β (TGF-β) signaling and downregulated ECM proteins such as type I collagen [26, 27]. Nintedanib also inhibited macrophage activation and reduced the number of M2 macrophages in the model of systemic sclerosis [28].

Nintedanib has shown broad-spectrum activity against receptor and non-receptor tyrosine kinases and blocks various signaling cascades. Thus, in addition to direct inhibition of lung fibroblasts, it is expected to have multiple effects on other tissues in the lung. In this study, we investigated whether treatment with nintedanib resulted in improvement of histopathological symptoms in iRA-ILD mice.

Materials and Methods

Animal Care and Use

D1CC×D1BC mice were produced by mating D1CC and D1BC transgenic mice and breeding in a pathogen-free animal care facility of Nagoya City University Medical School, according to the guidelines of the facility.

Induction of inflammatory arthritis and nintedanib administration

Inflammatory polyarthritis was induced as previously described [6, 7]. Briefly, mice were anesthetized with isoflurane and immunized with bColII (0.01 mg/mouse) with an equal volume of complete (1^{st}) and incomplete (2^{nd}-5^{th}) Freund's adjuvant. The first immunization was given 8 to 10 weeks after birth. The mice were monitored by scoring the joints. Nintedanib was dissolved in 0.5% methylcellulose and administered daily (90 mg/kg) by oral gavage from weeks 35 to 43 after the 1^{st} immunization (Figure 1A). Serum samples were collected from the jugular vein at week 43. The right lobe of the lung was used for histopathological analysis and the left lobe was used for Western blotting.

ELISA

Quantitation of serum SP-D (Yamasa, Japan) and RF IgG and IgM (Fujifilm Wako Shibayagi, Japan) concentrations were determined using ELISA according to the manufacturer's instructions. DBA, D1CC, and D1BC mice were used as controls. The cut-off value of serum SP-D was 53.9 ng/mL and was evaluated in a laboratory study [8].

Multiplex cytokine assay

The Bio-Plex Mouse Cytokine 8-Plex (Bio-Rad) was used to quantify the concentration of serum cytokines (IL-1β, IL-2, IL-4, IL-5, IL-10, GM-CSF, IFN-γ, and TNFα). The assay was performed according to the manufacturer's instructions.

Serum AST and ALT

Serum AST and ALT levels were quantified using the transaminase Cii test (Wako, Japan) according to the manufacturer's instructions.

Histopathology and Immunohistochemistry

The lungs were euthanized, harvested, and fixed with 4% paraformaldehyde diluted in PBS. Paraffin sections (2 μm) were stained with hematoxylin-eosin (HE), Masson's trichrome, and the following primary antibodies for immunohistochemistry: rabbit anti-E-cadherin, rabbit anti-αSMA, rabbit anti-vimentin, rabbit anti-MMP7 (Cell Signaling

Technology), rabbit anti-SP-C (Hycult Biotech), rat anti-Podoplanin (MBL), rabbit anti-collagen I (Novus Biologicals), rat anti-F4/80 (Bio-Rad), rabbit anti-CD3 (Genemed Biotechnologies), rat anti-PTPRC/CD45R (Aviva Systems Biology), rabbit anti-arginase I (GeneTex), mouse anti-peptidyl-citrulline (F95) and rabbit anti-S100A4 (Millipore), and mouse anti-Laminin γ2 N-terminal fragment (γ2pf, Funakoshi). Histofine Simple Stain Mouse MAX-PO secondary antibodies (Nichirei) and the Opal 4-color Fluorescent IHC kit (PerkinElmer) were used according to the manufacturer's protocol. All images were captured by fluorescence microscopy (BZ-X710, Keyence) and analyzed by hybrid cell count (Keyence) or Fiji.

Western Blotting

Western blotting (WB) analysis was performed using the ECL system. The following primary antibodies were used: rabbit anti-PDGFRα, rabbit anti-PDGFRβ (Cell Signaling Technology), rabbit anti-Pad4 (MBL), rabbit anti-SP-C (Hycult Biotech), goat anti-SP-D (R&D Systems), rabbit anti-COL1A1 (Boster biological technology), rabbit anti-SP-A, and mouse anti-tubulin-α (Santa Cruz) antibodies. Statistical analysis of the expression levels of each protein was performed using Fiji.

***In situ* hybridization**

In situ hybridization for *Scgb1a1, Sftpc*, *Col1a1, Tgf-β, Krt5, Krt17, Padi2,* and *Padi4* was performed using the RNAscope Multiplex Fluorescent Reagent Kit v2 (Advanced Cell Diagnostics), according to the manufacturer's instructions.

Statistical analyses

The results are shown as mean ± S.E. The significance of differences between vehicle, nintedanib, and age-matched control was calculated by one-way analysis of variance followed by Dunnett's test for multiple comparisons. Student's *t*-test was used to analyze the AST and ALT levels in the serum, as shown in Supplemental figure 2. A value of $p < 0.05$ was considered statistically significant.

Results

D1CC×D1BC mouse has high susceptibility to RA-ILD

Approximately 96% of D1CC×D1BC mice underwent severe joint inflammation after 1st immunization with low-dose bColII (Supplemental figure 1A). Although most D1CC$^{+/-}$ mice showed chronic and slow disease progression [6], 70% of D1CC×D1BC mice showed acute severe swelling and redness of the entire paw from the initial onset (Supplemental Table 1).

Serum concentrations of RF IgG and IgM in D1CC×D1BC, D1CC, D1BC mice, and their genetic background DBA/1J were measured as controls. Serum RF levels in D1CC×D1BC mice were higher than those in single transgenic or DBA/1J mice, even in the absence of stimulation with the arthritogenic antigen (Supplemental Table 2). High serum RF levels suggest that D1CC×D1BC mice are more susceptible to joint inflammation than single transgenic mice. In contrast, serum SP-D as an ILD biomarker did not differ. The onset of ILD was determined by increased serum SP-D levels (> 53.9 ng/mL) from approximately 35 weeks after bColII immunization (Supplemental Table 1 and Supplemental figure 1B). Therefore, this increase in serum SP-D indicates the progression of lung fibrosis in D1CC×D1BC mice [8, 21].

Nintedanib reduced the incidence of ILD

We examined whether nintedanib attenuated arthritis-associated ILD. The oral administration of nintedanib or vehicle was started from 35 weeks after the first immunization and continued daily for 2 months (Figure 1A). The incidence of IP determined by serum SP-D above the cut-off was approximately 65% in bColII immunized D1CC×D1BC mice (hereafter, this induced-RA-ILD mouse model is referred to as iRA-ILD) (Figure 1B). Administration of nintedanib decreased the incidence of IP (Figure 1B). However, this effect was not reflected in the mean serum concentration of SP-D (Figure 1C). The disease progression in iRA-ILD mice was slower than expected and no deaths occurred during this study. Mortality was the same for both vehicle- and nintedanib-treated iRA-ILD mice (Supplemental figure 2A). No adverse liver effects were observed in D1CC×D1BC mice treated with nintedanib (Supplemental figure 2B-D).

Next, we studied histopathological features using antibodies against E-cadherin (epithelial bronchiole), podoplanin (type I alveolar epithelial cells, AEC1), and SP-C (type 2 alveolar epithelial cells, AEC2). Metaplastic bronchioles, hyperplastic AEC2, and punctured podoplanin-positive areas were observed in the vehicle; however, these features were remodeled by nintedanib treatment (Figure 1D and 1E). We also analyzed

the expression of surfactant proteins A, C, and D in the whole lung by WB. Administration of nintedanib reduced the protein levels of these surfactant proteins (Figure 1F-H).

Nintedanib suppressed fibrosis and ColI accumulation

First, to confirm whether nintedanib administration suppressed fibrosis, Masson's trichrome-positive areas (blue stained regions) were analyzed by ImageJ as a fibrotic area. Nintedanib reduced the proportion of fibrotic area (Figure 2A and B). For further analysis of ECM deposition, type I collagen (Col1)- and αSMA-positive areas were calculated from immunohistochemical staining, showing a reduction in both positive areas (Figure 2C to E). The expression level of type I collagen in the whole lung was restored by nintedanib (Figure 2F). As nintedanib inhibits the signaling cascade of PDGFR, we also examined whether nintedanib alters the expression levels of PDGFRα and PDGFRβ in the lung. The expression level did not vary with nintedanib administration (Figure 2G and H). Therefore, administration of nintedanib attenuates pulmonary fibrosis associated with ECM deposition in iRA-ILD mice.

The number of M2 macrophages was decreased by nintedanib

As the histopathological features of iRA-ILD mice represent NSIP-like pathological features, we studied infiltrated lymphocytes in the lung. Alveolar macrophages tended to polarize M2 rather than M1 phenotype in pulmonary fibrosis [29]. The number of infiltrated macrophages (F4/80), arginase I and F4/80 positive M2 macrophages, B cells (CD45R), and T cells (CD3), were counted in the lung by immunohistochemical staining (Figure 3). Only the number of M2 macrophages was decreased by nintedanib, suggesting that the effect of nintedanib is associated with polarization from M2- to M1-macrophage (Figure 3C to F). Next, we compared serum cytokine levels in nintedanib- or vehicle-treated iRA-ILD mice. Most M2 macrophage-related serum cytokines, such as IL-4, 5, and 10, were slightly reduced. Levels of M1 macrophage-related cytokines other than IFN-γ were similar or slightly decreased (Supplemental figure 3).

Nintedanib suppressed ILD-related epithelial abnormalities

To confirm the histopathological characterization of metaplastic epithelial cells (Figure 1E), we stained these cells with antibodies against E-cadherin (epithelial cells) and EMT-related marker, S100A4. E-cadherin and S100A4 double-positive cells were a minor population. E-cadherin-single positive epithelial cells, E-cadherin, and S100A4 double-positive cells were eliminated by nintedanib (Figure 4A). Immunohistochemical staining with antibodies against E-cadherin, γ2pf, and MMP7 was performed to determine whether

metaplastic cells acquired invasiveness. E-cadherin positive cells, including metaplastic cells, expressed MMP7; however, most metaplastic cells also expressed γ2pf simultaneously (Figure 4B). We concluded that these metaplastic cells migrate from respiratory bronchioles along with degradation of laminin at the basement membrane by metalloproteases such as MMP7 (hereafter, these metastatic cells named invasive epithelial cells) [30]. Thus, nintedanib suppressed the development of invasive epithelial cells. *In situ* hybridization was also performed for the expression of *Sftpc*, *Scgb1a1,* and a basal cell marker*, Krt5* (Supplemental figure 4). *Scgb1a1*-positive invasive epithelial cells were distinguished from *Sftpc*-positive hyperplastic ACE2s (Figure 4C). Most *Scgb1a1*-positive invasive epithelial cells and *Sftpc*-positive hyperplastic ACE2s vanished with nintedanib treatment, but no overt effects for *Sftpc*- and *Scgb1a1*-positive bronchioalveolar stem cells (in the square of the nintedanib-treated specimen, Figure 4C).

Expression of *Padi4* and *Padi2* was reduced in epithelial cells by nintedanib

TGF-β is expressed in alveolar macrophages and epithelial cells in IPF. A recent study of single cell analysis also demonstrated that *Tgfβ* and *collagen* are expressed in epithelial cells [31]. We tested the expression of *Tgf-β* and *Collagen1a1* (*Col1a1*) along with *Scgb1a1* in the lung. Both signals were detected in respiratory bronchioles and invasive epithelial cells in iRA-ILD mice (Figure 5A and Supplemental Figure 5). The expression of *Padi4* in these respiratory epithelia was also examined. As autoantibodies, such as ACPA are associated with the clinical evidence of RA-ILD, alveolar epithelial cells are plausible producers of citrullinated peptide [32]. Interestingly, *Padi2* and *Padi4* were detected in both respiratory epithelia and invasive epithelial cells (Figure 5B). Only *Padi4* was expressed in the respiratory epithelium at week 0, but not in DBA1/J mice, suggesting that *Padi4* expression was upregulated in D1CC×D1BC mice. (Supplementary Figure 6). Recently, a similar characteristic basaloid cell, which expresses *COL1A1*, *MMP7*, but no *Krt5*, was identified by single cell analysis [33, 34]. Since aberrant basaloid cells were uniquely expressed *KRT17*, we investigated whether *Padi4*-positive cell express *Krt17*. We identified *Padi4*-, K*rt17*-positive invasive population in vehicle, but there is no double positive population in nintedanib-treated mice and age-matched control (Figure 5C). Nintedanib reduced the expression of *Padi4* in the respiratory epithelium. Moreover, nintedanib also decreased citrullinated peptides (Figure 5D). To further confirm the expression of Pad4 in the whole lung, we performed WB. The expression of Pad4 was reduced by the administration of nintedanib (Figure 5E).

Discussion

A novel iRA-ILD model using D1CC×D1BC mice developed NSIP with partial UIP as a histopathological feature. Anti-fibrotic nintedanib suppressed fibrosis and eliminated invasive epithelial cells. Finally, nintedanib reduced the expression of Pad4 and citrullinated peptides in the lung, resulting in the suppression of EMT in epithelial cells.

The inflammatory arthritis model is described in conventional animal models such as collagen-induced arthritis; however, it does not reflect chronic symptoms seen in RA and pulmonary fibrosis as a complication. In this study, we demonstrated that chronic progressive joint disorder and subsequent pulmonary fibrosis were observed in more than 60% of D1CC×D1BC mice. There was no upregulation of serum SP-D levels during inflammatory arthritis. The pathogenic mechanisms of RA-ILD are poorly understood, but high levels of serum RF IgG and IgM, and anti-citrullinated protein antibodies may function as plausible risk factors for the development of ILD [30]. D1CC×D1BC mice may be highly susceptible to developing RA-ILD because of de novo citrullinated peptide by PADs in the respiratory epithelium. Nintedanib reduced the expression of *Padi2, Padi4, and* citrullinated peptides in the respiratory epithelium. This may reduce the production of target peptides by ACPA. The direct effects of nintedanib on antibody-producing plasma B cells have not yet been described, so details of biochemical and pathological studies on the production of ACPA are needed. This helps clarify the intervention via ACPA between RA and subsequent ILD.

Nintedanib reduced the number of infiltrated M2 macrophages and inhibited M2 polarization. Adhesion via type I collagen activates PI3K, followed by phosphorylation of Akt, which causes M2 macrophage polarization. This effect was attenuated by the PI3K inhibitor [35]. Nintedanib has been shown to reduce phospho-Akt expression [36] and may result in a decrease in the number of M2 macrophages. Thus, the anti-inflammatory effects of nintedanib could suppress fibrosis by inhibiting the production of Th2 cytokines via M2 macrophages. Serum cytokines, including Th2 cytokines, were reduced marginally. To this end, we should measure cytokines in bronchioalveolar ravage (BAL), but not in serum. However, measurement of cytokines in BAL and histopathological analysis is technically incompatible, which is a limitation of our study.

Complex pathological features in ILD lead to various histopathological classifications, suggesting that a single patient has a mixed pattern of UIP and NSIP [37]. Invasive epithelial cells were observed in the iRA-ILD mouse model. At this time, no morphological tumorigenic epithelial cells were found, except for acquired some EMT-related features such as the expression of *Col1a1*and *Tgf-β*. We also observed that some invasive epithelial cells were *Padi4*- and *Krt17*-positive. Further research will elucidate

the potential for EMT-mediated tumorigenesis and its relation to aberrant basaloid cells in the iRA-ILD model. The therapeutic effects of nintedanib on these epithelial cells are controversial, [38, 39] but nintedanib is a potent inhibitor of tumorigenesis by blocking the expression of EMT-related molecules *Tgf-β*, *Padi2,* and *Padi4* in respiratory epithelia.

Various functional blockages by nintedanib against invasive epithelial cells, respiratory epithelia, and M2 macrophages as well as fibroblasts, may suppress lung fibrosis. This is because nintedanib has a wide range of inhibitory effects on the development of RA-ILD. In fact, structure-based analysis and kinetic inhibition assay by nintedanib result in the blockade of at least 34 kinases, including PDGFR, FGFR, and VEGFR. There are also various inhibitory activities for epithelial cell related-kinases such as Abl1, Kit, TRAK, and Ret. Genome-scale analysis of lung cancer also identified a couple of prognostic biomarkers including kinases [40]. Inhibitors of these various kinases have the potential to be therapeutic agents for RA-ILD.

The effects of nintedanib extends not only to fibroblasts but also to macrophages and epithelial cells, resulting in reducing the overall symptoms of ILD in the mouse model. These evidences may support improved treatment in patients with RA-ILD, as nintedanib acts as a broad inhibitory effect on many tyrosine kinases.

Figure legends

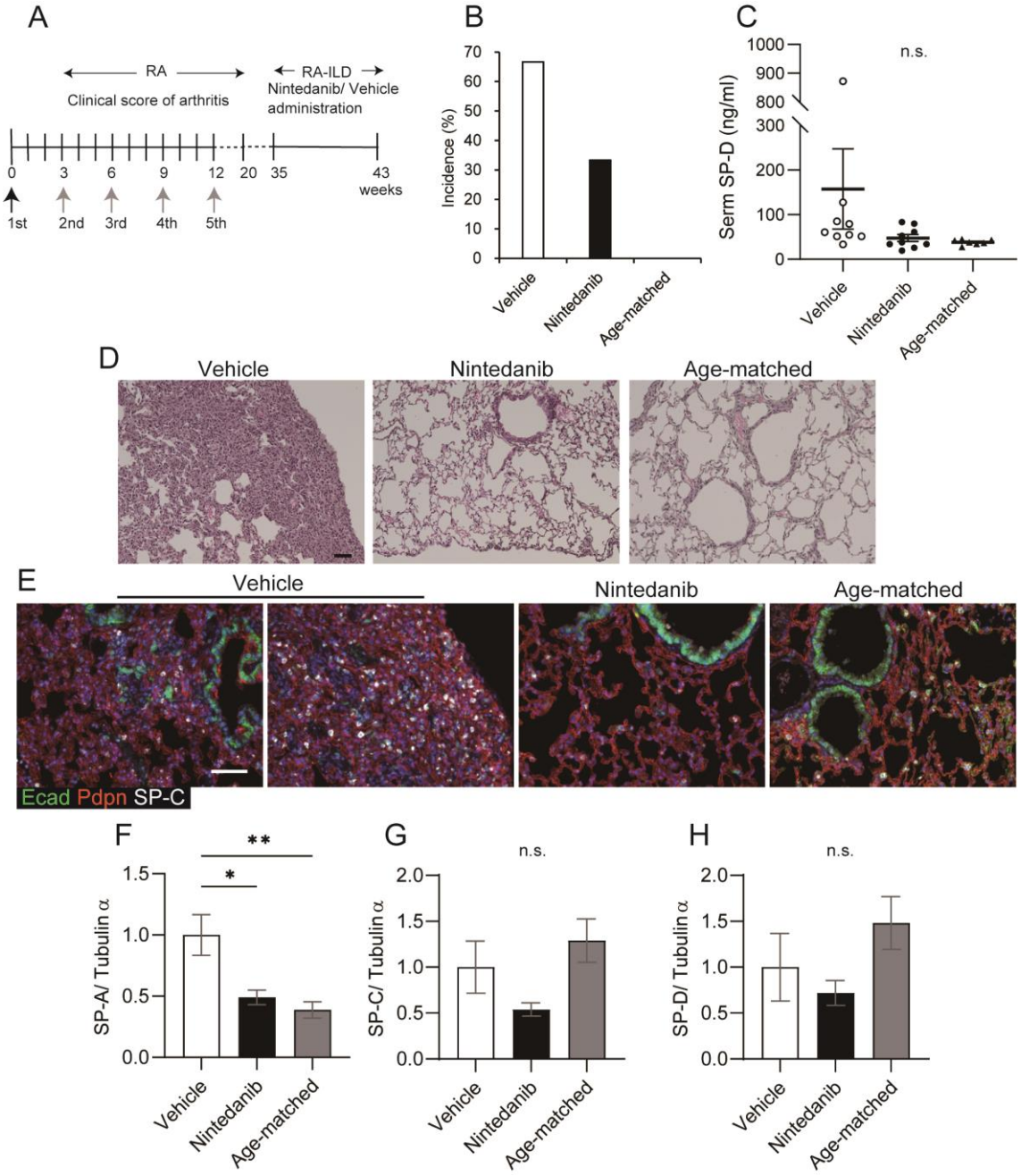

Figure 1 Nintedanib attenuates development of ILD after inflammatory arthritis

(A) The schematic diagram shows the time course of bColII immunization and the oral administration of nintedanib, which is done daily for two months from 35 weeks after 1st immunization. Arrows indicate ColII immunization (black: bColII/complete Freund's Adjuvant, gray: bColII/Incomplete Freund's Adjuvant). (B) The incidence of ILD is determined by overall cut-off of serum SP-D (>53.9 ng/ml) at 43 weeks after the 1st

immunization of bColII of nine mice in each group. (C) Serum SP-D levels are measured at 43 weeks after 1st immunization of bColII. Data are presented as mean ± S.E. of nine mice for each group (A-C). Each symbol represents vehicle (black circle), nintedanib (black square), and age-matched control (black triangle), respectively. (D-E) Histopathology by HE staining (D) and triple immunohistochemical staining for podoplanin (Pdpn, red), E-cadherin (Ecad, green), and SP-C (white) are performed in vehicle, nintedanib-treated, or age matched control mice (E). Scale bars indicate 50 μm (black and white). (F-H) The expression of SP-A (F), -C (G), and -D (H) in the lung tissue is assessed by WB. Data are presented as mean ± S.E. of four mice for each group. Asterisk indicates $*P < 0.05$, $**P < 0.001$, compared with vehicle group. n.s., non-significant.

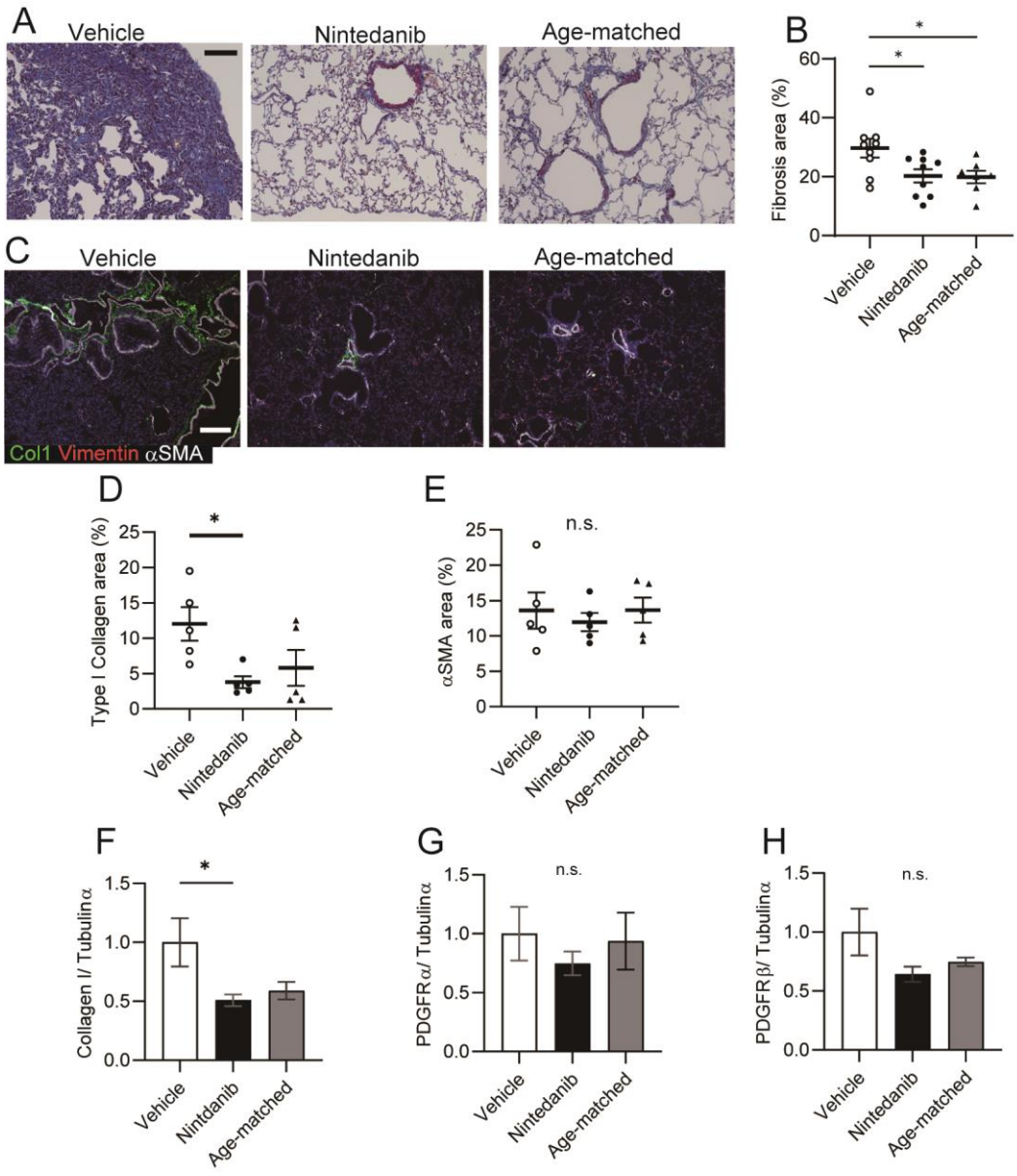

Figure 2 Nintedanib attenuates lung fibrosis

(A) Masson's trichrome staining for vehicle, nintedanib-administrated, or age matched lung specimen. (B) All images for the section from left lung and accessory lobe, are captured at a magnification of 200×, and blue fibrotic areas for the total lung areas are calculated by Fiji. Data are presented as mean ± S.E. of nine mice for each group. (C) Immunohistochemical staining for type I collagen (Col1, green), vimentin (red), and αSMA (white). Scale bars indicate 100 μm (white and black). (D-E) Type I collagen (D) and αSMA (E) expressing areas in left lung and accessory lobe are calculated by Fiji. The calculation of stained-images is done as same as in (B). Data are presented as mean ± S.E. of five mice for each group. (F-H) Type I collagen (F), PDGFRα (G) and -Rβ (H) in the

whole lung tissues are assessed by WB. Data are presented as mean ± S.E. of four mice for each group. Asterisk indicates $*P < 0.05$ compared with vehicle group. n.s., non-significant.

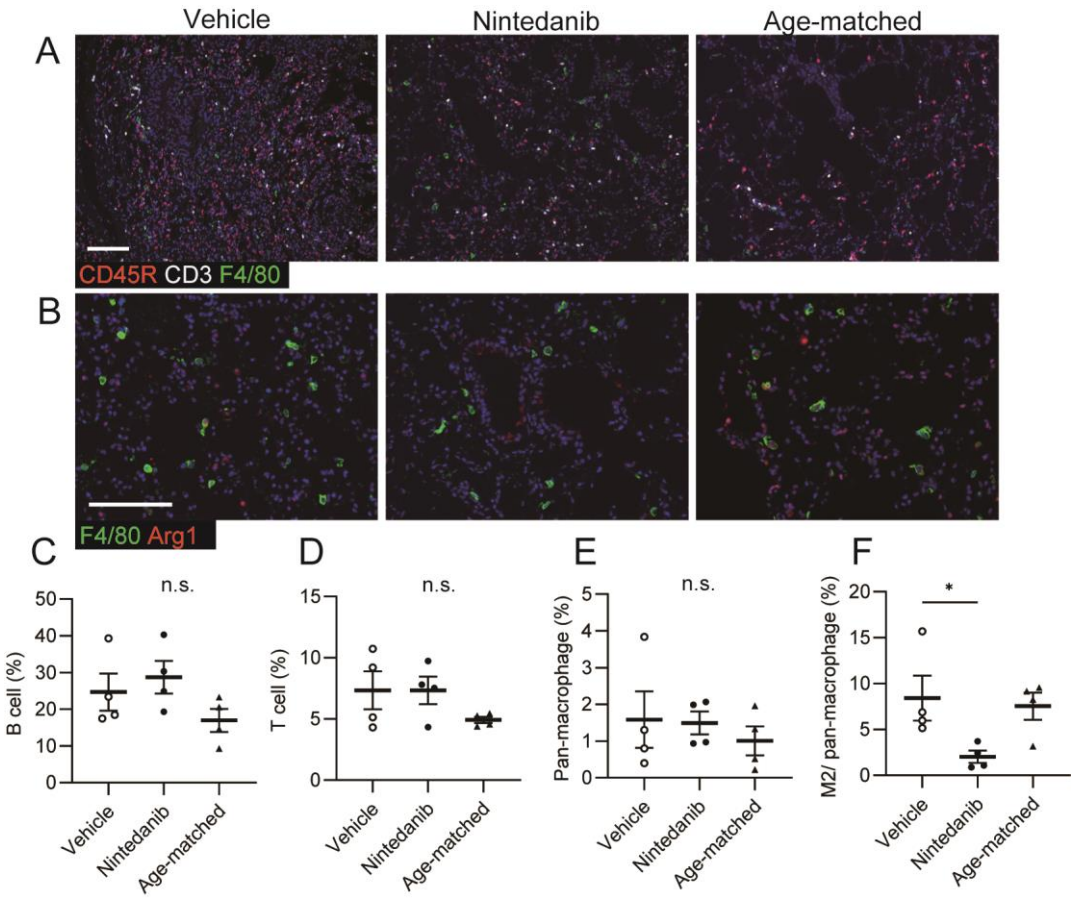

Figure 3 M2 macrophage polarization was suppressed by nintedanib treatment

(A-B) Immunohistochemical staining for F4/80 (green), CD45R (red), and CD3 (white) (A), F4/80 (green) and arginase I (red) (B). Scale bars indicate 50 μm. (C-F) The percentage of each infiltrated lymphoid cell is calculated. B cells (C), T cells (D), pan macrophages (E), and the ratio of M2 macrophage in pan-macrophages (F). Images from each immunohistochemical staining in left lung and accessory lobe, which are captured at a magnification of 100× and calculated the ratio of each lymphoid cell for total nuclear cells by Fiji or M2 macrophages in pan-macrophages by hybrid cell count. All data are presented as mean ± S.E. of four mice in each group. Asterisk indicates $*P < 0.05$ compared with vehicle group. n.s., non-significant.

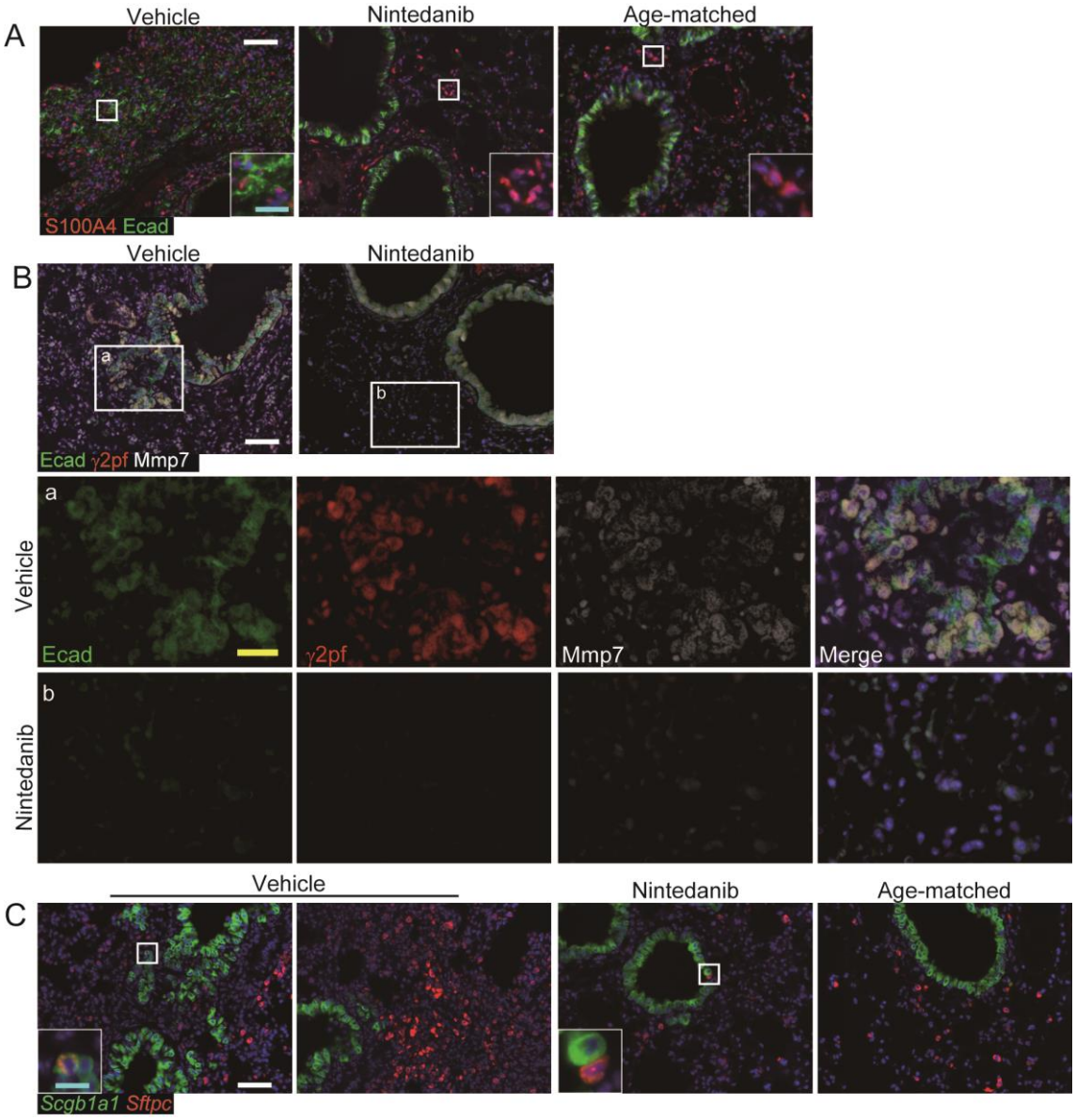

Figure 4 Nintedanib suppressed the development of invasive epithelial cells and hyperplastic AEC2

(A) Immunohistochemical analysis using E-cadherin (Ecad, green) and S100A4 (red). S100A4 single positive cells are estimated as fibroblasts and lymphoid cells including T cells and macrophages. (B) Immunohistochemical analysis using E-cadherin (Ecad, green), γ2pf (red), and MMP7 (white). Invasive epithelial cells secrete MMP7 and degrade laminin (a). The administration of nintedanib suppressed the occurrence of these invasive epithelial cells (b). (C) *In situ* hybridization is performed using *Scgb1a1* (green) and *Sftpc* (red). Most *Scgb1a1-positive* invasive epithelium do not express *Sftpc* simultaneously. No overt effect by nintedanib on a limited number of *Scgb1a1* and *Sftpc*-

positive BASCs is observed (square in vehicle). Scale bars indicate 50 μm (white), 20 μm (yellow), and 10 μm (cyan).

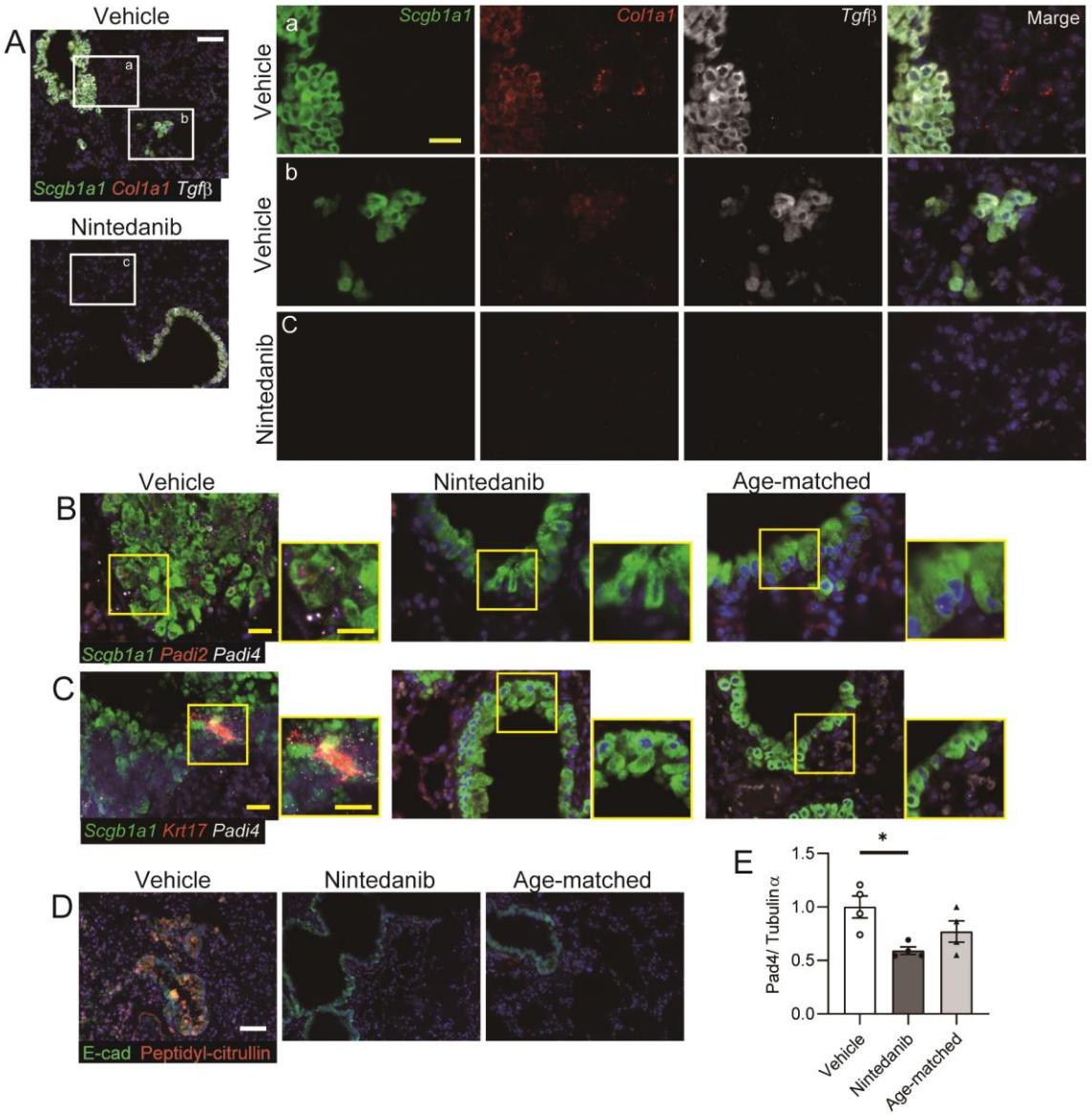

Figure 5 Nintedanib suppressed the expression of *Padi4* and the production of citrullinated peptide in respiratory epithelia

(A) *In situ* hybridization of *Scgb1a1* (green), *Tgf-β* (white), and *Col1a1* (red). *Tgf-β* and *Col1a1* express in both alveolar epithelium and invasive epithelial cells. As nintedanib suppressed the occurrence of invasive epithelial cells, *Tgf-β* and *Col1a1*-positive invasive cells are not observed. (B and C) *In situ* hybridization of *Scgb1a1* (green), *Padi4* (white), and *Padi2* or *Krt17* (red). *Padi4* and *Padi2* expression is reduced in nintedanib treatment. (D) Immunohistochemical analysis using E-cadherin (Ecad, green) and peptidyl-citrulline (red) in vehicle- or nintedanib-treated and age-matched mouse lungs. Scale bars indicate 50 μm (white) and 20 μm (yellow). (E) The expression of Pad4 in the lung tissues is

assessed by WB. Data are presented as mean ± S.E. of four mice for each group. Asterisk indicates *$P < 0.05$ compared with vehicle group.

Online supplementary materials have been separated.

Acknowledgments

We thank Dr. Makoto Murata for his cooperation in measuring serum SP-D and Dr. Stefan-Lutz Wollin for useful discussions. We also thank Boehringer Ingelheim Pharma GmbH & Co. KG for supplying nintedanib. We would like to thank Editage (www.editage.com) for English language editing.

DISCLOSURE STATEMENT

Grant support: This work was supported by grants-in aid from the Ministry of Education, Culture, Sports, Science and Technology (MEXT)/JSPS KAKENHI Grant Number JP 26461470, 23591444, 17K09982, and 17K16055, research grant from Nagoya City University Grant Number 1943005.

Contributors: SK and HO were involved in the design of the study. YM, HO, and SK were involved in data acquisition and the analysis. All authors were involved in the interpretation of the data, drafted the final version of the manuscript.

Competing interests: SK and HO received research support from Boehringer Ingelheim Pharma GmbH & Co. KG. SK received personal donation from T. Furuya.

Patient consent for publication: Not required.

Ethics approval: All mouse experiments were performed according to the rules and regulations of the Fundamental Guidelines for Proper Conduct of Animal Experiment and Related Activities in Academic Research Institutions under the jurisdiction of the Ministry of Education, Culture, Sports, Science and Technology Japan and approved by the committee on the ethics of Animal Experiments of Nagoya City University.

ORCID iD: YM 0000-0002-9324-8018, HO 0000-0002-8538-1150, AN 0000-0003-4947-4760, and SK 0000-0003-0690-0993

References

1. Gochuico BR, Avila NA, Chow CK, Novero LJ, Wu HP, Ren P, MacDonald SD, Travis WD, Stylianou MP, Rosas IO. Progressive preclinical interstitial lung disease in rheumatoid arthritis. *Archives of internal medicine* 2008: 168(2): 159-166.
2. Paulin F, Doyle TJ, Fletcher EA, Ascherman DP, Rosas IO. Rheumatoid Arthritis-Associated Interstitial Lung Disease and Idiopathic Pulmonary Fibrosis: Shared Mechanistic and Phenotypic Traits Suggest Overlapping Disease Mechanisms. *Rev Invest Clin* 2015: 67(5): 280-286.
3. Olson AL, Swigris JJ, Sprunger DB, Fischer A, Fernandez-Perez ER, Solomon J, Murphy J, Cohen M, Raghu G, Brown KK. Rheumatoid arthritis-interstitial lung disease-associated mortality. *American journal of respiratory and critical care medicine* 2011: 183(3): 372-378.
4. Bongartz T, Cantaert T, Atkins SR, Harle P, Myers JL, Turesson C, Ryu JH, Baeten D, Matteson EL. Citrullination in extra-articular manifestations of rheumatoid arthritis. *Rheumatology* 2007: 46(1): 70-75.
5. Keith RC, Powers JL, Redente EF, Sergew A, Martin RJ, Gizinski A, Holers VM, Sakaguchi S, Riches DW. A novel model of rheumatoid arthritis-associated interstitial lung disease in SKG mice. *Experimental lung research* 2012: 38(2): 55-66.
6. Kanazawa S, Ota S, Sekine C, Tada T, Otsuka T, Okamoto T, Sonderstrup G, Peterlin BM. Aberrant MHC class II expression in mouse joints leads to arthritis with extraarticular manifestations similar to rheumatoid arthritis. *Proceedings of the National Academy of Sciences of the United States of America* 2006: 103(39): 14465-14470.
7. Miura Y, Ota S, Peterlin M, McDevitt G, Kanazawa S. A Subpopulation of Synovial Fibroblasts Leads to Osteochondrogenesis in a Mouse Model of Chronic Inflammatory Rheumatoid Arthritis. *JBMR Plus* 2019: 3(6): e10132.
8. Terasaki Y, Terasaki M, Kanazawa S, Kokuho N, Urushiyama H, Kajimoto Y, Kunugi S, Maruyama M, Akimoto T, Miura Y, Igarashi T, Ohsawa I, Shimizu A. Effect of H2 treatment in a mouse model of rheumatoid arthritis-associated interstitial lung disease. *J Cell Mol Med* 2019: 23(10): 7043-7053.
9. Miura Y, Lam M, Bourke JE, Kanazawa S. Bimodal fibrosis in a novel mouse model of bleomycin-induced usual interstitial pneumonia. *bioRxiv* 2021: 2021.2003.2018.435059.
10. Lingampalli N, Sokolove J, Lahey LJ, Edison JD, Gilliland WR, Holers VM, Deane KD, Robinson WH. Combination of anti-citrullinated protein antibodies and rheumatoid factor is associated with increased systemic inflammatory mediators and more rapid progression from preclinical to clinical rheumatoid arthritis. *Clin Immunol*

2018: 195: 119-126.
11. Chen J, Doyle TJ, Liu Y, Aggarwal R, Wang X, Shi Y, Ge SX, Huang H, Lin Q, Liu W, Cai Y, Koontz D, Fuhrman CR, Golzarri MF, Liu Y, Hatabu H, Nishino M, Araki T, Dellaripa PF, Oddis CV, Rosas IO, Ascherman DP. Biomarkers of rheumatoid arthritis-associated interstitial lung disease. *Arthritis & rheumatology* 2015: 67(1): 28-38.
12. Kalluri R, Weinberg RA. The basics of epithelial-mesenchymal transition. *The Journal of clinical investigation* 2009: 119(6): 1420-1428.
13. Raghu G, Remy-Jardin M, Myers JL, Richeldi L, Ryerson CJ, Lederer DJ, Behr J, Cottin V, Danoff SK, Morell F, Flaherty KR, Wells A, Martinez FJ, Azuma A, Bice TJ, Bouros D, Brown KK, Collard HR, Duggal A, Galvin L, Inoue Y, Jenkins RG, Johkoh T, Kazerooni EA, Kitaichi M, Knight SL, Mansour G, Nicholson AG, Pipavath SNJ, Buendia-Roldan I, Selman M, Travis WD, Walsh S, Wilson KC, American Thoracic Society ERSJRS, Latin American Thoracic S. Diagnosis of Idiopathic Pulmonary Fibrosis. An Official ATS/ERS/JRS/ALAT Clinical Practice Guideline. *American journal of respiratory and critical care medicine* 2018: 198(5): e44-e68.
14. Kim KK, Kugler MC, Wolters PJ, Robillard L, Galvez MG, Brumwell AN, Sheppard D, Chapman HA. Alveolar epithelial cell mesenchymal transition develops in vivo during pulmonary fibrosis and is regulated by the extracellular matrix. *Proceedings of the National Academy of Sciences of the United States of America* 2006: 103(35): 13180-13185.
15. Selman M, Pardo A. Role of epithelial cells in idiopathic pulmonary fibrosis: from innocent targets to serial killers. *Proc Am Thorac Soc* 2006: 3(4): 364-372.
16. Stadler SC, Vincent CT, Fedorov VD, Patsialou A, Cherrington BD, Wakshlag JJ, Mohanan S, Zee BM, Zhang X, Garcia BA, Condeelis JS, Brown AM, Coonrod SA, Allis CD. Dysregulation of PAD4-mediated citrullination of nuclear GSK3beta activates TGF-beta signaling and induces epithelial-to-mesenchymal transition in breast cancer cells. *Proceedings of the National Academy of Sciences of the United States of America* 2013: 110(29): 11851-11856.
17. Liu M, Qu Y, Teng X, Xing Y, Li D, Li C, Cai L. PADI4mediated epithelialmesenchymal transition in lung cancer cells. *Mol Med Rep* 2019: 19(4): 3087-3094.
18. Chang X, Han J. Expression of peptidylarginine deiminase type 4 (PAD4) in various tumors. *Mol Carcinog* 2006: 45(3): 183-196.
19. Mutua V, Gershwin LJ. A Review of Neutrophil Extracellular Traps (NETs) in Disease: Potential Anti-NETs Therapeutics. *Clinical reviews in allergy & immunology* 2020.

20. Liu L, Zhang Z, Zhang G, Wang T, Ma Y, Guo W. Down-regulation of PADI2 prevents proliferation and epithelial-mesenchymal transition in ovarian cancer through inhibiting JAK2/STAT3 pathway in vitro and in vivo, alone or in combination with Olaparib. *J Transl Med* 2020: 18(1): 357.
21. Flaherty KR, Wells AU, Cottin V, Devaraj A, Walsh SLF, Inoue Y, Richeldi L, Kolb M, Tetzlaff K, Stowasser S, Coeck C, Clerisme-Beaty E, Rosenstock B, Quaresma M, Haeufel T, Goeldner RG, Schlenker-Herceg R, Brown KK, Investigators IT. Nintedanib in Progressive Fibrosing Interstitial Lung Diseases. *The New England journal of medicine* 2019: 381(18): 1718-1727.
22. Hilberg F, Roth GJ, Krssak M, Kautschitsch S, Sommergruber W, Tontsch-Grunt U, Garin-Chesa P, Bader G, Zoephel A, Quant J, Heckel A, Rettig WJ. BIBF 1120: triple angiokinase inhibitor with sustained receptor blockade and good antitumor efficacy. *Cancer research* 2008: 68(12): 4774-4782.
23. Richeldi L, du Bois RM, Raghu G, Azuma A, Brown KK, Costabel U, Cottin V, Flaherty KR, Hansell DM, Inoue Y, Kim DS, Kolb M, Nicholson AG, Noble PW, Selman M, Taniguchi H, Brun M, Le Maulf F, Girard M, Stowasser S, Schlenker-Herceg R, Disse B, Collard HR, Investigators IT. Efficacy and safety of nintedanib in idiopathic pulmonary fibrosis. *The New England journal of medicine* 2014: 370(22): 2071-2082.
24. Wollin L, Distler JHW, Redente EF, Riches DWH, Stowasser S, Schlenker-Herceg R, Maher TM, Kolb M. Potential of nintedanib in treatment of progressive fibrosing interstitial lung diseases. *The European respiratory journal : official journal of the European Society for Clinical Respiratory Physiology* 2019: 54(3).
25. Redente EF, Aguilar MA, Black BP, Edelman BL, Bahadur AN, Humphries SM, Lynch DA, Wollin L, Riches DWH. Nintedanib reduces pulmonary fibrosis in a model of rheumatoid arthritis-associated interstitial lung disease. *American journal of physiology Lung cellular and molecular physiology* 2018: 314(6): L998-L1009.
26. Rangarajan S, Kurundkar A, Kurundkar D, Bernard K, Sanders YY, Ding Q, Antony VB, Zhang J, Zmijewski J, Thannickal VJ. Novel Mechanisms for the Antifibrotic Action of Nintedanib. *American journal of respiratory cell and molecular biology* 2016: 54(1): 51-59.
27. Huang J, Beyer C, Palumbo-Zerr K, Zhang Y, Ramming A, Distler A, Gelse K, Distler O, Schett G, Wollin L, Distler JH. Nintedanib inhibits fibroblast activation and ameliorates fibrosis in preclinical models of systemic sclerosis. *Annals of the rheumatic diseases* 2016: 75(5): 883-890.
28. Huang J, Maier C, Zhang Y, Soare A, Dees C, Beyer C, Harre U, Chen CW, Distler O, Schett G, Wollin L, Distler JHW. Nintedanib inhibits macrophage activation

and ameliorates vascular and fibrotic manifestations in the Fra2 mouse model of systemic sclerosis. *Annals of the rheumatic diseases* 2017: 76(11): 1941-1948.

29. Pechkovsky DV, Prasse A, Kollert F, Engel KM, Dentler J, Luttmann W, Friedrich K, Muller-Quernheim J, Zissel G. Alternatively activated alveolar macrophages in pulmonary fibrosis-mediator production and intracellular signal transduction. *Clin Immunol* 2010: 137(1): 89-101.

30. Doyle TJ, Patel AS, Hatabu H, Nishino M, Wu G, Osorio JC, Golzarri MF, Traslosheros A, Chu SG, Frits ML, Iannaccone CK, Koontz D, Fuhrman C, Weinblatt ME, El-Chemaly SY, Washko GR, Hunninghake GM, Choi AM, Dellaripa PF, Oddis CV, Shadick NA, Ascherman DP, Rosas IO. Detection of Rheumatoid Arthritis-Interstitial Lung Disease Is Enhanced by Serum Biomarkers. *American journal of respiratory and critical care medicine* 2015: 191(12): 1403-1412.

31. Xu Y, Mizuno T, Sridharan A, Du Y, Guo M, Tang J, Wikenheiser-Brokamp KA, Perl AT, Funari VA, Gokey JJ, Stripp BR, Whitsett JA. Single-cell RNA sequencing identifies diverse roles of epithelial cells in idiopathic pulmonary fibrosis. *JCI Insight* 2016: 1(20): e90558.

32. Zeng J, Xu H, Fan PZ, Xie J, He J, Yu J, Gu X, Zhang CJ. Kaempferol blocks neutrophil extracellular traps formation and reduces tumour metastasis by inhibiting ROS-PAD4 pathway. *J Cell Mol Med* 2020: 24(13): 7590-7599.

33. Adams TS, Schupp JC, Poli S, Ayaub EA, Neumark N, Ahangari F, Chu SG, Raby BA, DeIuliis G, Januszyk M, Duan Q, Arnett HA, Siddiqui A, Washko GR, Homer R, Yan X, Rosas IO, Kaminski N. Single-cell RNA-seq reveals ectopic and aberrant lung-resident cell populations in idiopathic pulmonary fibrosis. *Sci Adv* 2020: 6(28): eaba1983.

34. Habermann AC, Gutierrez AJ, Bui LT, Yahn SL, Winters NI, Calvi CL, Peter L, Chung MI, Taylor CJ, Jetter C, Raju L, Roberson J, Ding G, Wood L, Sucre JMS, Richmond BW, Serezani AP, McDonnell WJ, Mallal SB, Bacchetta MJ, Loyd JE, Shaver CM, Ware LB, Bremner R, Walia R, Blackwell TS, Banovich NE, Kropski JA. Single-cell RNA sequencing reveals profibrotic roles of distinct epithelial and mesenchymal lineages in pulmonary fibrosis. *Sci Adv* 2020: 6(28): eaba1972.

35. Stahl M, Schupp J, Jager B, Schmid M, Zissel G, Muller-Quernheim J, Prasse A. Lung collagens perpetuate pulmonary fibrosis via CD204 and M2 macrophage activation. *PloS one* 2013: 8(11): e81382.

36. Wollin L, Maillet I, Quesniaux V, Holweg A, Ryffel B. Antifibrotic and anti-inflammatory activity of the tyrosine kinase inhibitor nintedanib in experimental models of lung fibrosis. *The Journal of pharmacology and experimental therapeutics* 2014: 349(2): 209-220.

37. Yamakawa H, Sato S, Tsumiyama E, Nishizawa T, Kawabe R, Oba T, Kamikawa T, Horikoshi M, Akasaka K, Amano M, Kuwano K, Matsushima H. Predictive factors of mortality in rheumatoid arthritis-associated interstitial lung disease analysed by modified HRCT classification of idiopathic pulmonary fibrosis according to the 2018 ATS/ERS/JRS/ALAT criteria. *J Thorac Dis* 2019: 11(12): 5247-5257.
38. Hostettler KE, Zhong J, Papakonstantinou E, Karakiulakis G, Tamm M, Seidel P, Sun Q, Mandal J, Lardinois D, Lambers C, Roth M. Anti-fibrotic effects of nintedanib in lung fibroblasts derived from patients with idiopathic pulmonary fibrosis. *Respir Res* 2014: 15: 157.
39. Wollin L, Wex E, Pautsch A, Schnapp G, Hostettler KE, Stowasser S, Kolb M. Mode of action of nintedanib in the treatment of idiopathic pulmonary fibrosis. *The European respiratory journal : official journal of the European Society for Clinical Respiratory Physiology* 2015: 45(5): 1434-1445.
40. Shi YX, Yin JY, Shen Y, Zhang W, Zhou HH, Liu ZQ. Genome-scale analysis identifies NEK2, DLGAP5 and ECT2 as promising diagnostic and prognostic biomarkers in human lung cancer. *Scientific reports* 2017: 7(1): 8072.

Suppression of epithelial abnormalities by nintedanib in induced-rheumatoid arthritis-interstitial lung disease mouse model

Yoko Miura[1], Hirotsugu Ohkubo[2], Akio Niimi[2], and Satoshi Kanazawa[1]

Author affiliations

[1] Department of Neurodevelopmental Disorder Genetics, Nagoya City University Graduate School of Medical Sciences, Nagoya, Japan.

[2] Department of Respiratory Medicine, Allergy and Clinical Immunology, Nagoya City University Graduate School of Medical Sciences, Nagoya, Japan.

Supplemental Materials

Supplemental Figures

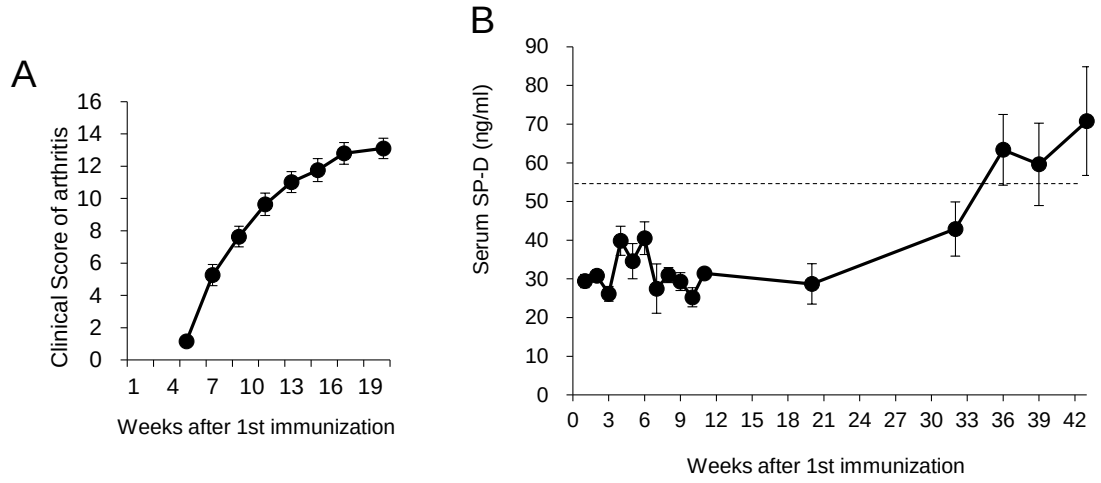

Supplemental figure 1. Interstitial pneumonia following severe inflammatory arthritis in D1CC×D1BC mice

(A) Mice are immunized with a low dose bColII five times every 3 weeks. The clinical score of the joins was evaluated. Data are presented as means ± S.E. of twenty mice. (B) Serum SP-D levels are increased about 35 weeks after the 1st immunization. Data are presented as means ± S.E. of thirteen mice. The dashed line indicates the cut-off of serum SP-D (53.9 ng/mL).

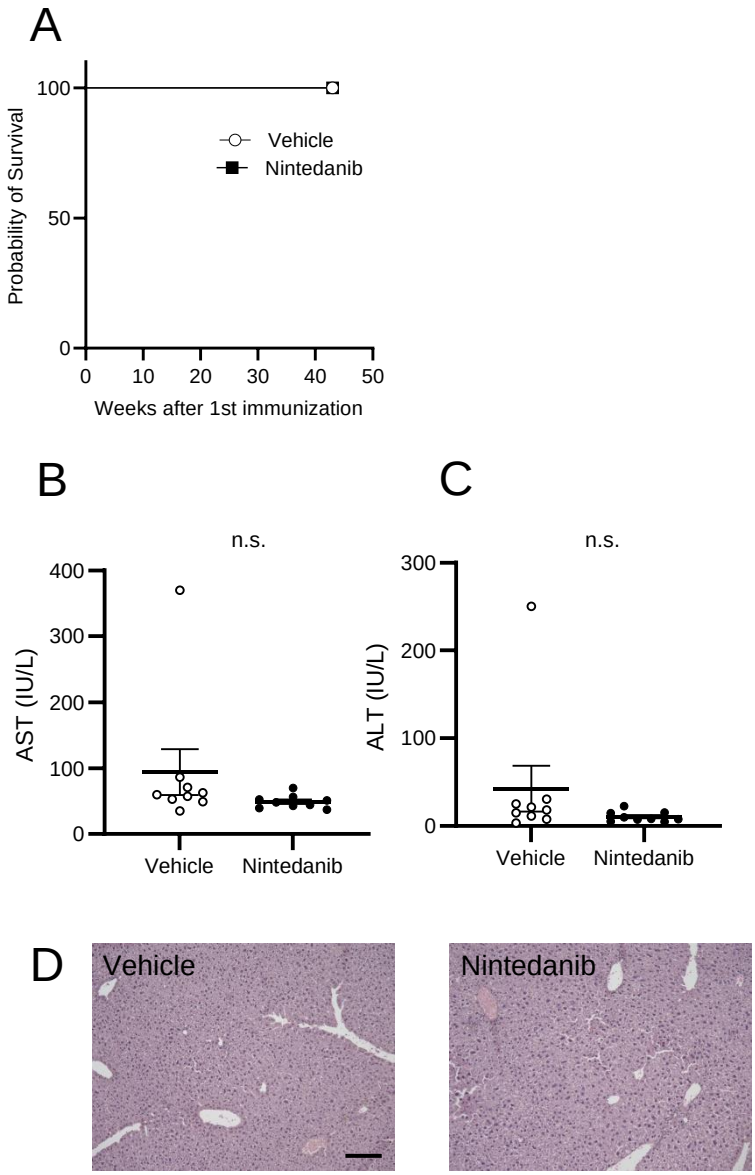

Supplemental figure 2. **No adverse effects of nintedanib-treatment in iRA-ILD mice**
(A) Kaplan-Meier analysis of mortality in iRA-ILD mice treated with nintedanib. (B-C) The adverse effects of nintedanib are as high levels of AST and ALT in serum and diarrhea in patients with IPF. We confirmed whether nintedanib had adverse effects on serum AST B) and ALT (C). Data are presented as mean ± S.E. of nine mice for each group. n.s., non-significant. (D) Histopathology (HE) of the liver of vehicle - or nintedanib-treated mice. Scale bar indicates 50 μm.

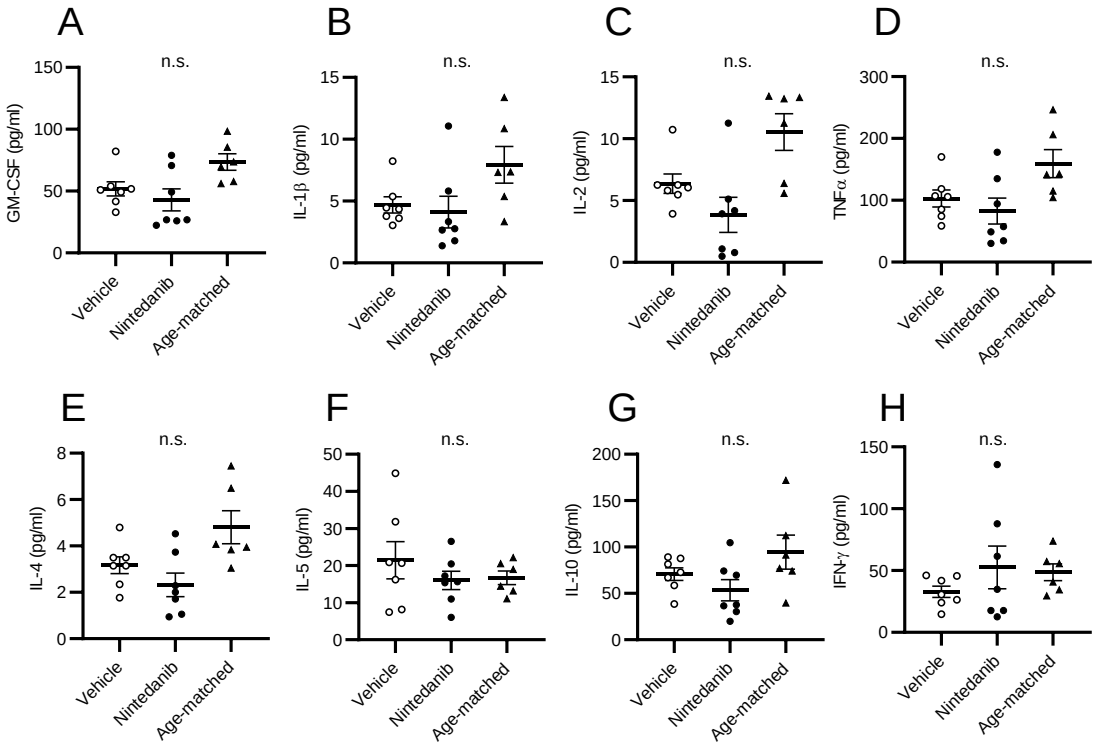

Supplemental figure 3. Nintedanib suppressed serum Th2 cytokines

Various serum cytokines, including GM-CSF (A), IL-1β (B), IL-2 (C), TNFα (D), IL-4 (E), IL-5 (F), IL-10 (G), and IFN-γ (H) were measured using Multiplex (BioRad). Each symbol represents vehicle (black circle), nintedanib (black square), and age-matched control (black triangle), respectively. Data are presented as means ± S.E. of seven or six mice in each group. n.s., non-significant.

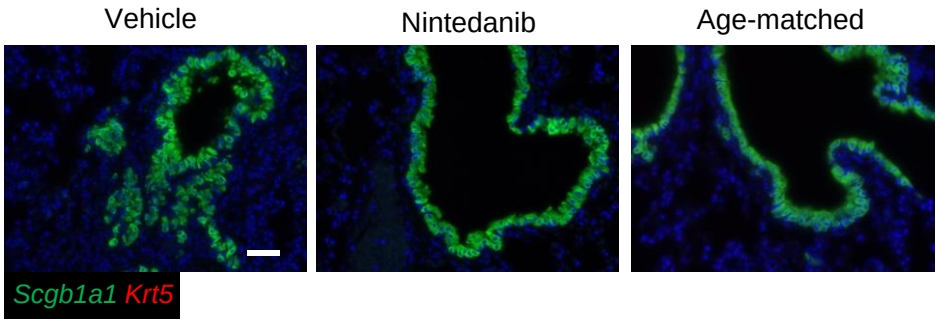

Supplemental figure 4. *Krt5* does not express in *Scgb1a1*-positive invasive epithelial cells

In situ hybridization of *Scgb1a1* (green) and *Krt5* (red) in vehicle- or nintedanib-treated mice and age-matched control mice. Scale bar indicates 20 μm.

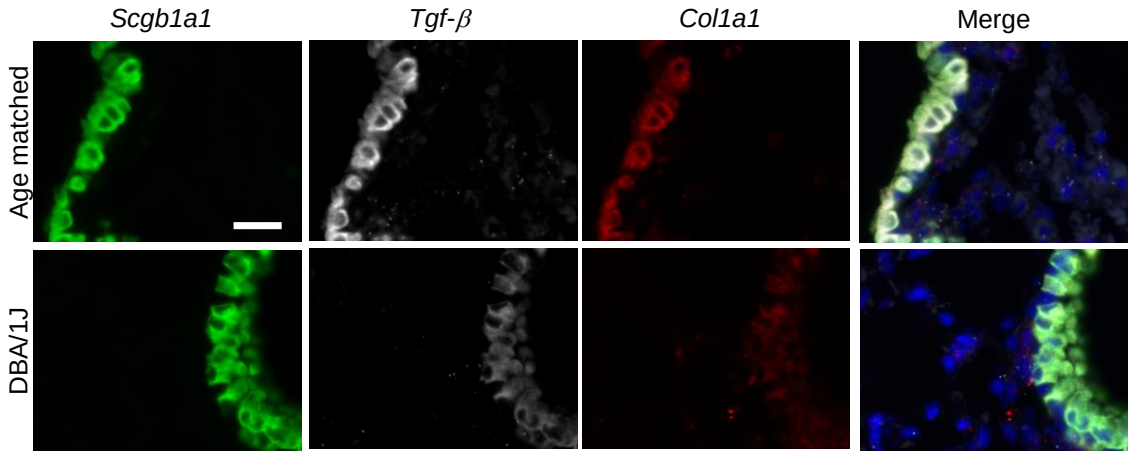

Supplemental figure 5. *Tgf-β* and *Col1a1*-positive invasive epithelial cells were not observed in age-matched control and DBA/1J mice

In situ hybridization of *Scgb1a1* (green), *Tgf-β* (white), and *Col1a1* (red). *Tgf-β* and *Col1a1* are expressed in both the alveolar epithelium and invasive epithelial cells in age-matched control and DBA/1J mice. Scale bar indicates 20 μm.

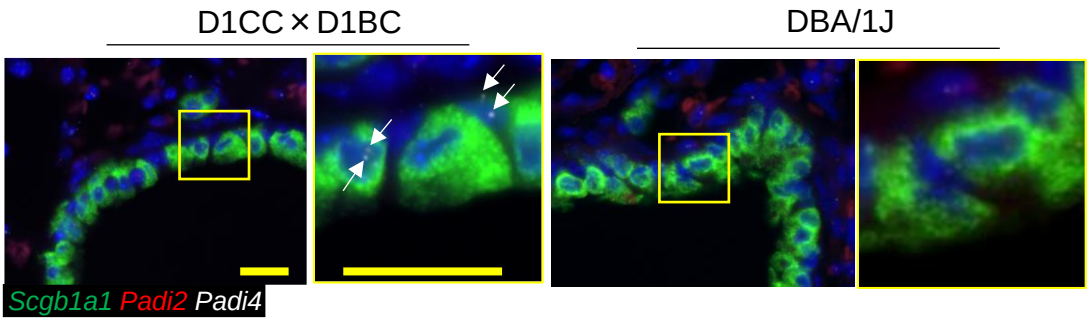

Supplemental figure 6. *Padi4* and *Padi2* expresses in alveolar epithelium

In situ hybridization of *Scgb1a1* (green), *Padi4* (white), and *Padi2* (red) mRNA expression in D1CC×D1BC and DBA/1J mice (week 0). White arrows indicate the signal of *Padi4*. Scale bar indicates 20 μm.

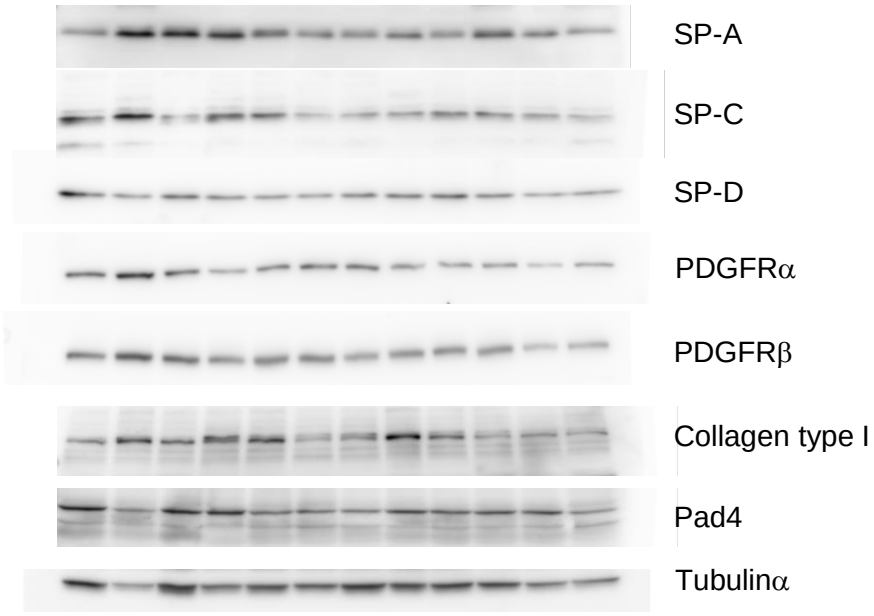

Supplemental figure 7

Protein expression in whole lung extracts determined by Western blot and visualized by the ECL chemiluminescence system. The relative signal intensity for each protein was determined using tubulin-α as a loading control (shown for one blot only, bottom). Details about antibodies have been provided in the Materials and Methods. Grouped data are shown in Figure 1F to 1H (SP-A, SP-C, and SP-D), Figure 2F to 2H (PDGFRα, PDGFRβ, and Collagen type I), and Figure 5D (Pad4).

Supplemental table 1. Difference of variability of clinical score in D1CC hetero (+/-) and D1CC×D1BC mice.

Mouse	Score 0 to 2 (%)	Score 0 to 3 (%)
$D1CC^{+/-}$	100	0
$D1CC^{+/+}\times D1BC^{+/+}$	30	70

Values show disease progression rates of arthritis in $D1CC^{+/-}$ and $D1CC^{+/+}\times D1BC^{+/+}$ mice. The clinical severity of arthritis was quantified for each limb according to a scoring system: 0 = no clinical symptoms; 1 = swelling and redness in one or two joints; 2 = moderate swelling and redness in more than three joints; 3 = severe swelling and redness of the entire paw. Data are presented as means ± S.E. of ten mice in each group.

Supplemental table 2. Comparison of the levels of RF IgG, IgM and SP-D in DBA/1J, D1CC, D1BC and D1CC×D1BC mice.

Mouse	RF IgG (mU/ml)	RF IgM (mU/ml)	SP-D (ng/ml)
DBA/1J	4501 ± 1040.5	6302 ± 1369.6	24.3 ± 2.29
$D1CC^{+/+}$	7342 ± 1137.6	12615 ± 1331.8	21.6 ± 1.87
$D1BC^{+/+}$	8074 ± 605.7	10767 ± 1084.1	31.4 ± 1.26
$D1CC^{+/+}\times D1BC^{+/+}$	12726 ± 2051.6*	24699 ± 3303.4*	21.2 ± 1.94

Data are presented as mean ± S.E. of more than five mice in each group. Asterisks show *P<0.05 compared with DBA/1J mice.